Fractures in heterogeneous two-dimensional systems

Antonio Politi[1,2,*] and Maria Zei[2,3,4,†]
[1]*Istituto Nazionale di Ottica Applicata, Largo E. Fermi 6 I-50125 Firenze, Italy*
[2]*Istituto Nazionale di Fisica della Materia, Unità di Firenze, Firenze, Italy*
[3]*Dipartimento di Meccanica e Tecnologie Industriali, Università di Firenze, Firenze, Italy*
[4]*Laboratoire de Physique, Ecole Normale Supérieure, Lyon, France*
(Received 5 July 2000; published 13 April 2001)

A two-dimensional triangular lattice with bond disorder is used as a testing ground for fracture behavior in heterogeneous materials in strain-controlled conditions. Simulations are performed with two interaction potentials (harmonic and Lennard-Jones types) and different breaking thresholds. We study the strain range where the fracture progressively develops from the first to the last breakdown. Scaling properties with the lattice size are investigated: no qualitative difference is found between the two interaction potentials. Clustering properties of the broken bonds are also studied by grouping them into disjoint sets of connected bonds. Finally, the role of kinetic energy is analyzed by comparing overdamped with dissipationless dynamics.

DOI: 10.1103/PhysRevE.63.056107 PACS number(s): 62.20.Mk, 62.20.Fe, 81.40.Jj, 81.40.Lm

I. INTRODUCTION

Understanding fracture dynamics is important not only for its practical applications but also because it represents a theoretical challenge to nonequilibrium statistical mechanics. The growing interest observed in recent years within the physics community has a multifold origin: (i) the ubiquity of fractal geometries in natural phenomena has represented a strong motivation for studying fractures [1]; (ii) the huge improvements in computer performance have made possible the execution of increasingly realistic simulations; (iii) the development of new experimental techniques has allowed accurate measurements over a wide range of scales [2,3]; (iv) the general expectation that statistical phenomena can be accommodated in a few universality classes has stimulated the formulation and study of many simplified models. The major difficulties for a realistic numerical study arise from the many different spatial (and temporal) scales involved in fracture dynamics, which range from the atomic scale to the macroscopic level. In fact, in some numerical studies, the tip of the fracture is treated quantum mechanically, while an intermediate region around the fracture itself is studied by integrating Newton's equations (with a suitable choice of the interaction potential), and, finally, the remaining part of the medium is treated as a continuum [4]. Additional difficulties arise from the existence of a large variety of materials which can be (i) more or less heterogeneous, depending on the type and amount of defects, and (ii) either brittle or plastic, depending on their response to the applied stress [5,6]. Furthermore, different types of fracture do exist (here we shall consider open-mode or, equivalently, mode-I fractures, where a traction is exerted on the boundaries, but two shear modes exist as well) and, last but not least, either the strain or the stress can be controlled.

The two main focus issues of fracture investigations are evolution, once the fracture has been initiated, and the statistical description of the final structure. While in the former context it is obvious that one cannot disregard the specificity of fractures in building meaningful dynamical models, in the latter case, we have assisted in the development of models only indirectly connected to fractures in the hope of nevertheless capturing the key ingredients. One prominent example is represented by the variety of papers devoted in the past to the breakdown of random fuse networks, often used as a reference for fractures [7].

However, in spite of increased interest, a systematic study is still lacking and many properties have not yet been thoroughly investigated. The object of the present study is somewhere between the two philosophies mentioned above. Inspired by some recent experimental studies, where the appearance of microcracks prior to the formation of the final breakdown has been investigated [8–11], here we study the progressive breakdown of a system.

In order to keep the computer time within an affordable range and yet allow a reliable statistical analysis, we have decided to limit ourselves to studying a two-dimensional triangular lattice with nearest-neighbor interactions [12,13]. For the mutual interactions, the so-called Born model [14] is often chosen, as it is numerically convenient and also allows working in the simpler framework of square lattices, as the corresponding Poisson modulus remains finite. Here, we have preferred to consider central forces since this is a more general choice (it reduces, under suitable approximatations, to the Born model [14]) and allows study of non-negligible deviations from equilibrium.

With respect to the force field, we have considered both harmonic and Lennard-Jones (LJ) types, as there is a qualitative difference between them. In the latter case, beyond the inflection point of the potential, larger strains correspond to decreasing stresses: this nonlinear effect is obviously lacking in the harmonic case.

As to the heterogeneity of the material, two different setups are typically adopted. On the one hand, disorder is introduced as a distribution of thresholds, i.e., of the distances above which a bond is irreversibly broken, while the bond strengths are assumed to be equal to one another (see, for

*Email address: politi@ino.it
†Email address: zei@ino.it

instance, Refs. [15–17]). On the other hand, disorder is sometimes introduced as a distribution of bond strengths with the thresholds chosen equal to one another [12,13]. The simplest such idealization is that of a dichotomic distribution, where each bond is either intact or cut from the very beginning (following Ref. [18], the initially missing bonds are defined as ''cut,'' while those that are removed during the fracturing process are defined as ''broken''). As pointed out in Ref. [16], this second setup is not formally different from the first, since it can also be viewed as a dichotomic distribution in the thresholds (set equal to either 0 or the same preassigned value). In practice, however, almost all the studies in the former context have been performed by assuming that the support of the distribution of thresholds extends from 0 to finite values: this implies that bonds start to break already for infinitesimal strains, while in the latter context there exists a critical strain below which the medium deforms reversibly with no crack. Here, we have preferred to adopt the second point of view as it appears more ''realistic'' to us, although the various approximations introduced at different levels of description are so many that this becomes almost a subjective issue.

The very first question that we have investigated is the behavior inside the strain range where microcracks are progressively generated, finding that its width is independent of the system size for both the harmonic spring and the LJ potential. This has been shown by monitoring both the stress and the cumulative density of broken bonds. Next we have looked at the distribution of broken bonds by classifying them into two groups: (i) those belonging to the major cluster (composed of both broken and cut bonds) that ultimately separates the lattice into two disconnected subsets; and (ii) those belonging to ''microscopic'' clusters generated away from the macroscopic fracture [19]. As a result, we find a different scaling behavior for the two classes, which suggests that in larger lattices the majority of bond breakdowns should occur out of the main crack.

Finally, we have studied the fracture scaling properties, by computing the ''length'' of the leading crack and of the microcracks. The standard way to characterize a fracture is through the roughness exponent ζ, which measures the scaling behavior of the transverse fluctuations of the fracture surface upon changing the longitudinal scale. An alternative approach is based on the computation of the fractal dimension D, which is connected to ζ by a simple relation that, in two dimensions, reads as $D=2\zeta$. In particular, we have tested the role of kinetic energy, by simulating an overdamped lattice. As a result, we have found that in this case the total number of broken bonds grows linearly with the system size. This disappearance of fractal features indicates that the kinetic energy is very important in determining the scaling properties. It would be desirable to verify whether the same holds true in other setups, where, e.g., the fracture has been grown by redetermining the stationary state each time a single bond has been broken.

More specifically, the next section is devoted to introducing the model and some of the notations. The third section, the core of the paper, deals with a thorough investigation of the harmonic potential, with the computation of several indicators. In Sec. IV, we discuss the dynamics of an overdamped lattice, while Sec. V is mainly devoted to comparing the results for the LJ potential with those for harmonic springs. Finally, in Sec. VI we discuss and summarize the implications of our analysis.

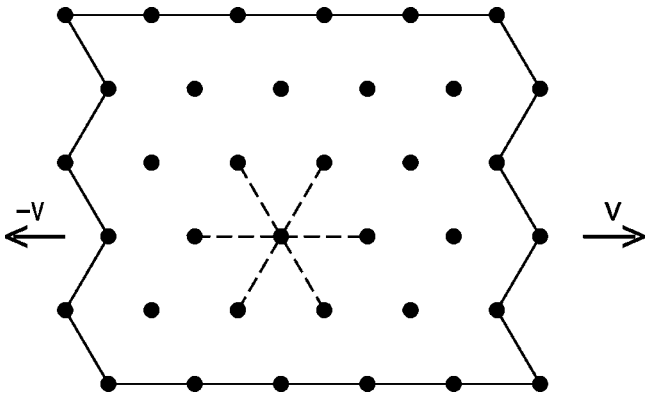

FIG. 1. Sketch of the triangular lattice. The dashed lines refer to the interactions involving a given site with its nearest neighbors. The left and right boundaries are pulled apart with velocity v. Free boundary conditions are assumed along the upper and lower borders.

II. MODEL

The model consists of a two-dimensional triangular lattice with nearest-neighbor interactions (see Fig. 1) that break as soon as the mutual distance becomes larger than a suitable threshold. In the bulk, the total force acting on a given atom is the sum of the contributions arising from the interaction with its six neighbors (see the dashed lines in Fig. 1).

More precisely, by denoting the position of the ith ''atom'' by $\vec{r}_i$, the force $\vec{f}_{ij}$ due to the interaction with the jth particle is written as

$$\vec{f}_{ij}=F(|\vec{r}_i-\vec{r}_j|)\frac{\vec{r}_i-\vec{r}_j}{|\vec{r}_i-\vec{r}_j|}, \tag{1}$$

where $|\cdot|$ represents the modulus operation and $F(u)$ is a scalar function defining the force law. Here, we have considered both linear, $F(u)=-\alpha(u-a)$ (harmonic case), and Lennard-Jones type forces,

$$F(u)=\frac{\alpha a}{6}\left[\left(\frac{a}{u}\right)^{13}-\left(\frac{a}{u}\right)^{7}\right], \tag{2}$$

where the parameters are fixed in such a way that $u=a$ is the equilibrium position in either case (i.e., a is the lattice spacing at rest), and to guarantee that the quadratic term of the LJ potential coincides with the harmonic potential. In order to explicitly eliminate the irrelevant parameters, we suitably rescale the spatial variable as well as the time axis: this allows getting rid of both α and a, which will be fixed equal to 1 for the rest of the paper (notice that the masses can also be scaled out). Accordingly, all the quantities studied in this paper are adimensional.

The critical threshold a^*, however, is a relevant parameter that cannot be scaled out. We have performed most of our numerical investigations for $a^*=1.1$, but some tests for larger thresholds ($a^*=1.5,1.8$) have been made as well. In the case of the LJ potential, we have fixed $a^*=1.8$, above the inflection point of the potential, in order to ensure a clear qualitative difference from the harmonic case.

The pulling process is actuated horizontally, by symmetrically shifting the leftmost and rightmost lattice sites (those connected by the solid thick lines in Fig. 1) with a velocity $\pm v$. The velocity has been chosen small enough to guarantee that the whole lattice remains nearly at equilibrium during the initial elastic deformation. Simulations performed with different velocities have allowed us to conclude that $v=10^{-4}$ is slow enough, so that we have selected such a value in all our studies.

Fixed boundary conditions have been imposed along the lateral borders (i.e., we studied strain-controlled fractures), while free boundary conditions have been chosen along the upper and lower borders (see again Fig. 1). This is a simple way to reproduce the conditions imposed in some experiments (see, for instance, [20]).

A local dissipation, i.e., a force term $-\gamma\dot{\vec{r}}_i$, has been added along the left and right boundaries, where we expect that the coupling with the external world is more effective in removing kinetic energy from the medium. It is, in fact, necessary to include some dissipation to prevent the transformation of potential energy into kinetic energy due to the progressive bond breaking leading to an unrealistic amount of kinetic energy traveling all over the lattice. This is a similar choice to that made when performing numerical simulations of heat conductivity in lattice systems, where the only atoms coupled with the heat baths are those on the oppositive boundaries [21]. The only exception to this setup has been made in Sec. IV where, in order to test the role of kinetic energy, we added a dissipation term on all sites.

The equations of motion have been integrated by using a leapfrog algorithm that allows preserving the Hamiltonian structure in the bulk and easily adding the dissipation wherever required. The time step has been fixed equal to 10^{-2}.

The last important ingredient of the model is the disorder. We have chosen to work with two types of bond: intact ones characterized by the same spring constant $\alpha=1$ and cut ones characterized by $\alpha=0$. Accordingly, the fraction c of initially missing bonds represents an indicator of disorder. For $c=0$ we have a perfectly homogeneous lattice. It is well known that $c=c_p\equiv 0.65(3)$ is the ordinary percolation threshold, i.e., for $c>c_p$ there are so many missing bonds that the lattice is no longer macroscopically connected [22]. Moreover, in the case of central forces, there is a second threshold, the so-called rigidity-percolation threshold ($c_r=0.3398$ [23]) above which the lattice, although connected, has zero Young modulus.

Preliminary numerical studies performed to test the correctness of our algorithms and the reliability of the model have revealed, e.g., that the propagation of fractures is correctly described with the onset of the typical velocity instabilities [24].

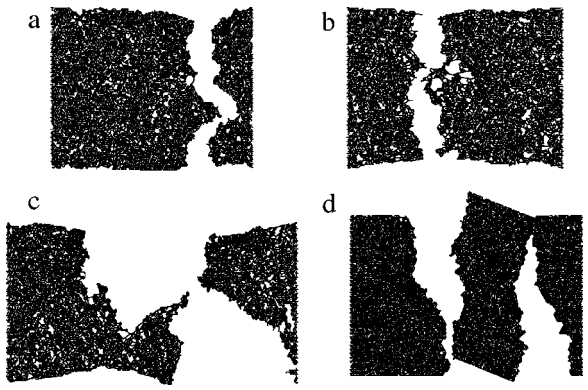

FIG. 2. Different instances of fractures in a lattice with linear size $L=80$: (a) Lennard-Jones potential with 30% of initially cut bonds; (b) harmonic potential, threshold equal to 1.1, 30% of cut bonds (simulation performed with no kinetic energy); (c) same as (b) with a different realization of the disorder and with kinetic energy; (d) Lennard-Jones potential and 15% of cut bonds.

All simulations have been performed in $L\times(L+1)$ lattices, i.e., in media with aspect ratio close to 1. Before discussing the quantitative results in the next section, let us here briefly illustrate the phenomenology that can be observed for some realizations of the disorder and for different choices of the interaction. For relatively small strains, the bond lengths remain below the breaking threshold. The inhomogeneities of this process are just determined by the initial distribution of cut bonds. Above some critical strain, microfractures arise in different regions of the lattice until the whole lattice is separated into at least two disconnected pieces by a macroscopic fracture. A typical example is reported in Fig. 2(a), where a rough fracture is clearly visible together with some small holes corresponding either to isolated microfractures or to initial clusters of missing bonds. The final structure can, however, be more complex, as illustrated in the other panels. In Fig. 2(b), the generation of almost macroscopic holes has accompanied the onset of the main fracture. In Fig. 2(c), one can see instead that the fracture initially followed two different routes which eventually connect after some twisting. Such a phenomenon is brought to an extremum in the example reported in Fig. 2(d), where one of the two paths eventually becomes dominant, leading to a partial overlap in the top right region. We can, in a sense, state that the stressless rotations allowed by the model make it good for reproducing the behavior of nearly two-dimensional objects embedded in a three-dimensional space like sheets of paper. It is also clear that these strong deformations, which are responsible for the final ductile behavior, make the system rather different from a random fuse network, where only the connectivity is important. Moreover, we want to remark that, occasionally, small fragments (composed of a few particles) detach, rapidly flying away, very much in analogy to what happens when, e.g., a glass breaks in real life. This represents the first qualitative indication of the relevance of kinetic energy in the whole process.

III. HARMONIC CASE

In this section we extensively discuss the fracturing process for the harmonic potential with the threshold set equal

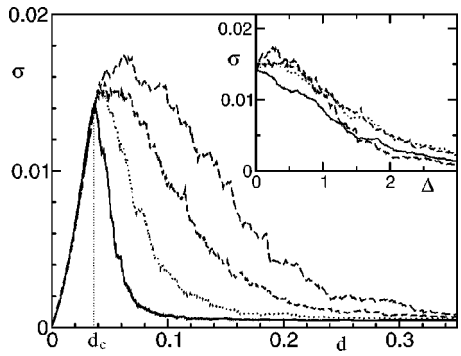

FIG. 3. Stress-strain curve in lattices of different dimension with harmonic potential, threshold equal to 1.1, and 30% of cut bonds. The long-dashed, dashed, dotted, and solid lines refer to $L=10$, 20, 40, and 80, respectively. In the inset, we report the same curves versus Δ, the unscaled strain after a suitable shift [see Eq. (4) with $d_c=0.0368$].

to $a^*=1.1$ and for a fraction of broken bonds $c=0.3$ close to but definitely below the rigidity-percolation threshold. We start from the stress-strain curves. The stress σ is defined as the horizontal (x) component of the force per unit length,

$$\sigma=\frac{1}{L}\sum |f_{ij}^{(x)}|, \tag{3}$$

where the sum extends to all bonds along one of the two edges where the stress is applied.

In Fig. 3 we report the stress averaged over 100 different realizations of the disorder as a function of the strain $d=D/L$ (where $D=vt$ is the overall stretch) for different lattice sizes ($L=10$, 20, 40, and 80). We have verified that the differences between the forces applied on the left and right sides are much smaller than the statistical deviations still observable after the averaging process.

The small-strain region is characterized by a nice scaling behavior: all curves perfectly overlap along a line that deviates significantly from a straight line behavior. In this strain range, the statistical uncertainty is rather small (less than 10^{-4} for all sizes). The nonlinear behavior of the load curve follows from the combined choice of (i) a large c value close to the rigidity-percolation threshold, so that the entire lattice has to be quite stretched before the microscopic strains overcome the preassigned threshold and (ii) a not-too-small critical elongation (0.1, compared, for instance, with the value chosen in Ref. [13], $a^*-1=10^{-4}$). The two circumstances combine to determine sizable lattice deformations which, in turn, contribute to stronger nonlinear effects. It is interesting to notice that we are not so close to the percolation threshold as to be affected by finite-size corrections associated with the phase transition.

The overlap appears to end at a critical strain d_c (see the vertical line in Fig. 3), above which the onset of microcracks leads to a rearrangement of the lattice to withstand the imposed strain and, eventually, gives rise to a decrease of the stress. This second regime characterized by the development of the fracture becomes shorter and shorter upon increasing the lattice size L. In order to establish the scaling behavior within what we call the fracture range, we introduce the variable

$$\Delta=(d-d_c)L, \tag{4}$$

which is basically the unscaled strain (dL) shifted by an amount proportional to the system size. The best data collapse was obtained for $d_c=0.0368$ (see the inset in Fig. 3). Its relatively low quality is due to both the large statistical fluctuations and the existence of finite-size corrections. In fact, on the one hand, the maximum statistical error on σ is equal to 1.5×10^{-3}, 8×10^{-4}, 5×10^{-4}, and 3×10^{-4} for $L=10$, 20, 40, and 80, respectively; on the other hand, one can see that the position of the maximum stress progressively shifts to the left, testifying to the non-negligible role of the finite size L. In any case, although a clear-cut conclusion cannot be drawn, the approximate data collapse suggests that the size of the fracture range is asymptotically independent of L.

In order to gain some further insight into the fracture process, we have looked at the dependence of the number of broken bonds $N(d)$ on the strain. Again, by considering d as the independent variable (as it is indeed so in the numerical experiment), we have averaged the fraction of broken bonds for fixed d,

$$n(d)=\frac{N(d)}{N_b} \tag{5}$$

(N_b is the final number of broken bonds in a given realization), over the different realizations of the disorder, obtaining $\langle n\rangle$. Notice that n is nothing but the cumulative distribution of broken bonds, i.e., the integral of the probability density $Q(\Delta)$ of broken bonds. The resulting behavior is reported in Fig. 4, again as a function of Δ (only the fracture range matters in this case). Except for the curve corresponding to the smallest size ($L=10$), there is a reasonably good data collapse: in fact, the deviations among the various curves are of the same order as the statistical uncertainty, which is approximately 2–3 %. These results confirm in a more convincing way that the strain range over which the whole fracture develops is independent of the system size. No significant difference is found if the fraction of broken bonds is fixed and the corresponding strain is averaged over the disorder realizations.

At this point, it is interesting to compare our findings with the previous knowledge on this type of systems. In particular, in Ref. [13], the behavior of the critical stress value σ_f for the breakdown of the first bond was extensively studied. The authors convincingly conjectured that $\sigma_f=(a+b\ln L)^{-\nu}$ with $0.5\leqslant\nu\leqslant1$. This result can be understood on the basis of the following simple observation: the typical size of the longest microcrack (due to the initial disorder) that can be found in a lattice of size L increases (logarithmically) with L. In particular, this is true for cuts perpendicular to the stress direction. The longer are such cuts, the more fragile is their tip. Accordingly, it is natural to expect that the minimal stress to break the first bond decreases with increasing L.

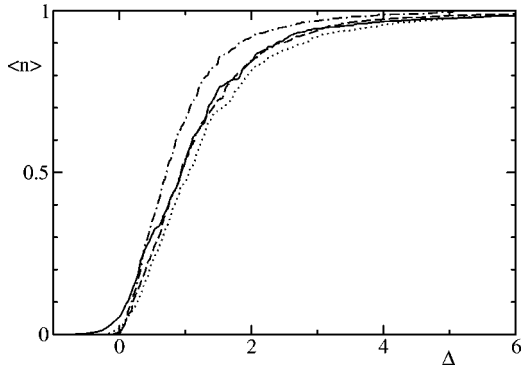

FIG. 4. Average number of broken bonds normalized to the final number N_b (i.e., cumulative probability distribution of broken bonds) as a function of Δ for the same physical setup as in Fig. 3. Dot-dashed, dashed, dotted, and solid lines refer to $L=10$, 20, 40, and 80, respectively.

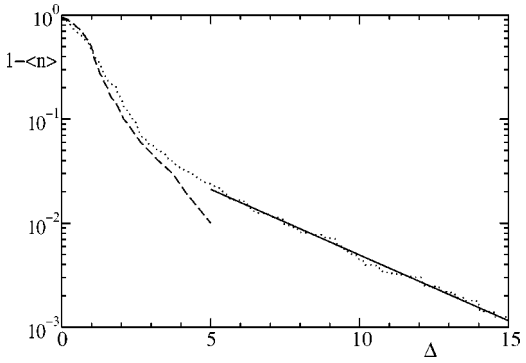

FIG. 5. Tail of the cumulative probability distribution of broken bonds for $L=80$. The dotted line refers to the average fraction of broken bonds for fixed d, while the dashed line is obtained by averaging the strains that correspond to the same fraction of broken bonds. Finally, the solid line with slope 0.3 represents the result of an exponential best fit. The large sample-to-sample fluctuations affecting the final stage of the fracture prevent a meaningful estimate of the statistical error.

We have tested this behavior in our simulations too. As sample-to-sample fluctuations of the strain turn out to be smaller than stress fluctuations, we have preferred to look at the behavior of the critical value of d_f (the nonperfect linear relationship linking d and σ is not a problem in regard to the scaling behavior, since the linear term remains predominant). By plotting $1/d_f$ versus $\ln L$, we find that the scaling law proposed in Ref. [13] holds true for this fairly large c value also (the largest concentration of missing bonds considered in Ref. [13] was $c=0.2$). Additionally, the exponent ν is more likely close to 1 than to 0.5. The above results can thus be interpreted by stating that the critical strain (or, equivalently, stress) for observing a finite fraction of bond breakings appears to remain finite even in the infinite L limit, while the critical strain value for observing the first break goes to zero. Altogether, the decrease of the critical strain with increasing L manifests itself as a tail in the underlying probability distribution $Q(\Delta)$ that extends to negative Δ values and, in principle, to $-\infty$ for $L\rightarrow\infty$.

A similar phenomenon is observed for large Δ values, i.e., corresponding to the final breakdown of the lattice. In this case, as the tail is much better pronounced, we can attempt a quantitative study. In Fig. 5 we report $1-\langle n\rangle$ versus Δ to investigate the convergence properties of the probability distribution. The dotted and dashed lines are the results of the avergage of n for fixed d and vice versa. We cannot say if the strong deviations observed for large Δ are real and reflect the sparse character of the last bond breakings, or if they are just due to a lack of statistics. In any case, with reference to the first curve, the solid line obtained with a best fit suggests the existence of an exponential tail.

Another interesting problem to be studied is the dependence of the total number of broken bonds $N_b(L)$ on the lattice size, with the aim of characterizing the possible fractal nature of the process. The data reported in Fig. 6 (see full circles) reveal a rather clean power law, $N_b \simeq L^{\beta}$. A best fit yields $\beta=1.35\pm0.03$. Considering that a macroscopic fracture cannot be shorter than a straight line, β must be larger than or equal to 1. It is important to understand whether the difference from 1 is to be attributed to the fractal structure of the main crack or to the distribution of microcracks. In order to clarify this point we decided to look more carefully at the spatial arrangement of the broken bonds. In Fig. 7(a) we report all broken bonds corresponding to the fracture process depicted in Fig. 2(a), indicating their spatial positions in the undeformed lattice. There, one can certainly see a large concentration of broken bonds around the region where the macroscopic fracture is eventually generated, but microcracks are distributed all over the lattice. We found it natural to group together cut and broken bonds into disjoint clusters of mutually connected bonds. The cluster ensemble obviously includes the major crack connecting the opposite edges of the lattice, together with a set of more or less microscopic clusters (the so-called precursors). The shape of the maximal cluster, including the cut bonds, is reported in Fig. 7(b) for the same realization of disorder as in Fig. 7(a).

Altogether, N_b is much smaller than the number N_c of cut bonds. This is not simply the consequence of our choice of a

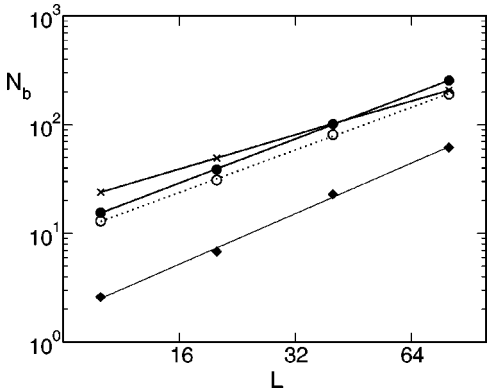

FIG. 6. Scaling behavior of the number of broken bonds for the harmonic potential with threshold equal to 1.1 and 30% of cut bonds. Full circles refer to the average total number of broken bonds; open circles refer to the broken bonds belonging to the leading cluster; diamonds refer to the broken bonds out of the leading cluster; crosses refer to the total number of broken bonds in the absence of kinetic energy.

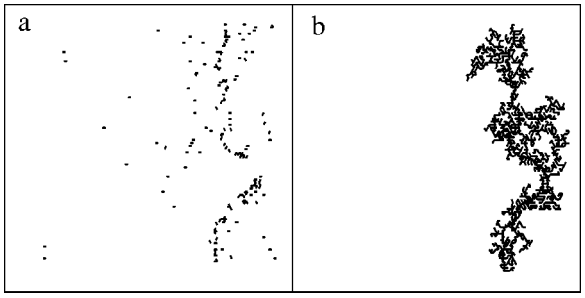

FIG. 7. Bonds broken during the fracture process with the same realization of disorder considered in Fig. 2(a). In (a), all broken bonds are reported with reference to the undeformed lattice. In (b), the whole leading cluster is reported, including broken and cut bonds.

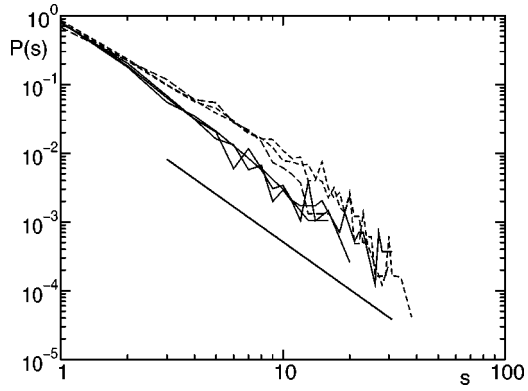

FIG. 8. Probability distribution of the cluster sizes of broken bonds in the harmonic potential for different lattice sizes, rescaled to the same maximum value (solid lines). The dashed lines represent the distributions that would be obtained by randomly adding broken bonds to the cut ones. The slope of the straight line is equal to -2.3.

relatively large c, but rather of the scaling behavior of N_b, which grows as $L^{1.35}$, while $N_c \approx L^2$ for any c value strictly larger than 0. However, although N_b is, for large L, negligible in comparison to N_c, the same appears not to be true within the maximal cluster: there, we found that the fraction of broken bonds remains finite for $L \to \infty$. This is not surprising, because, even though the fracture developed along an optimal path characterized by the maximal fraction of cut bonds, such a fraction must be strictly smaller than 1, as long as c remains below the percolation threshold, as here. In fact, in the present case, the fraction of bonds that are broken rather than cut in the maximal cluster is not smaller than 10%.

It is now instructive to separately investigate the scaling behavior of the numbers $N_b^{(i)}$ and $N_b^{(o)}$ of broken bonds inside and outside the maximal cluster, respectively. In Fig. 6, one can see that $N_b^{(i)}$ scales approximately in the same way as N_b (see the open circles, whose best fit yields $\beta = 1.31 \pm 0.03$), but this is an almost obvious consequence of the fact that $N_b^{(i)} \gg N_b^{(o)}$ (see the diamonds for the scaling behavior of $N_b^{(o)}$). More interesting is the growth rate exhibited by this latter class of bonds, which is definitely larger, $\beta = 1.52 \pm 0.06$. This result implies that, if the scaling behavior remains unchanged in yet larger lattices, the majority of broken bonds will be eventually found out of the main cluster.

It is thus important to understand how the broken bonds are distributed out of the main cluster. In particular, we would like to ascertain whether their $L^{1.5}$ growth is due to an increasing number of clusters, or to an increasing size of (a subset of) clusters. This can be clarified by looking at the probability distribution of cluster sizes. However, in order to perform a clean analysis, we have to get rid of the background composed of the cut bonds, which represent the vast majority of bonds belonging to the clusters. We decided to proceed as follows. For any given cluster (identified as such by simultaneously considering cut and broken bonds) we count the number s of broken bonds and define it as the cluster size. By then counting the number of clusters of different sizes over all realizations of disorder, we are in the position to compute the probability density $P(s)$. One should notice that this is different from the standard procedure usually adopted in the study of cluster distribution in random percolation [25]. The distributions for $L = 10$, 20, 40, and 80 are reported in Fig. 8 as solid lines: they are rescaled to start from the same value $P(1)$. The nice overlap indicates that the reason for the exponent 1.5 in the growth rate of $N_b^{(o)}$ is a homogeneous increase in the number of clusters of all sizes. Over the accessible range of s values, the cluster-size distribution approximately follows a power law with an exponent equal to -2.3 ± 0.1 (see the solid line in Fig. 8).

Finally, for the sake of comparison, we have investigated the difference from the simple case of a random cancellation of an equal number of bonds in addition to the cut bonds. The distributions obtained with this procedure correspond to the dashed lines in Fig. 8. The slower decay of this second group of curves (the slope is close to -2) is apparently counterintuitive: the bonds broken during the fracturing process are less clustered than those in the purely random process. In other words, it turns out that, once a bond is broken in a given cluster, it is less likely, rather than more likely, that further bonds will be broken in the same cluster. In fact, because of correlations in the local stress, small clusters grow by very little amounts, while only the leading cluster, the Griffith's crack, reaches the macroscopic scale.

As a further test, one could compare these results with the screened percolation model [26], in which case the randomly broken bonds are removed only from the backbone. However, no sizable differences can be expected in the regime that we have investigated, i.e., far from the percolation threshold.

IV. ROLE OF THE KINETIC ENERGY

In the previous section we extensively discussed some fracture properties in a given physical setup. We now start investigating the importance of some of the underlying assumptions. In this section we discuss the role of kinetic energy in determining the scaling properties of the broken bonds. In the past, while Newton's equations have been extensively used to simulate the propagation of fractures and to study the various instabilities occurring therein, they have

been less frequently employed in studying statistical properties of fractures.

Many papers (see, e.g., Ref. [16]) have dealt with models with a random distribution of thresholds, proposed as a natural extension of random fuse networks. By interpreting them as mesoscopic models, the role of dynamics has been reduced to guaranteeing an exponential convergence toward the instantaneous equilibrium configuration for the imposed (slowly varying) boundary conditions and the given set of mutual connections. A nontrivial evolution arises because, upon increasing either the stress or the strain, some local strains progressively overcome the allowed thresholds, thus imposing a continuous reequilibration of the system until the final breakdown is established.

In some other cases, intrinsic and extrinsic fluctuations have been included through the introduction of a stochastic rule [27–30]: in analogy to numerical studies of diffusion-limited aggregation, where particles are randomly added to the growing cluster, there, bonds have been randomly added to an initial crack with a suitable probability distribution.

In the present context, where the dissipation is acting only along the boundaries, it is not at all unlikely that the potential energy released from the breakdown of a given bond allows breaking further bonds, upon transforming itself into kinetic energy. It is much less obvious whether the number of broken bonds either increases or decreases. Indeed, on the one hand, we can predict that the kinetic energy facilitates the bond breaking along the leading crack, thereby reducing the stress on the bonds away from the critical region. If this is the scenario, the overall number of broken bonds should diminish. On the other hand, kinetic energy, transported through the lattice, might contribute to breaking all bonds that are nearly at threshold.

In order to find the true scenario, we have added a strong dissipation on each lattice site. The average number (again more than 100 different realizations of disorder) of broken bonds is reported in Fig. 6 (see the crosses) for the same L values as before. There, one can see that both of the above hypothesized mechanisms occur, since for small L N_b is larger than in the previous case, while the opposite is true for large L values. Altogether, this implies that N_b increases more slowly in the case of an overdamped motion. A best fit of the data in Fig. 6 yields an exponent $\beta = 1.04 \pm 0.05$. Within our accuracy, the growth is thus indistinguishable from a linear behavior (i.e., no fractality in the fracture process). While this is a clear indication that in the present context kinetic energy plays a crucial role in determining the scaling behavior of broken bonds, we should mention that in models with a random distribution of thresholds, fractal cracks are obtained even in the presence of overdamped dynamics [16,28]. This, however, does not exclude the possibility that even in such conditions different fractal dimensions might be obtained upon including the effect of kinetic energy.

Finally, let us comment on another element of agreement with previous studies. In Ref. [15], it was found that, whenever the distribution of thresholds was limited to a range of strictly positive values, nonfractal behavior for the fracture was observed. This is consistent with our findings, as the dynamical rule was based on a (potential) energy minimization.

V. FURTHER TESTS

Besides the extensive studies performed for $c = 0.3$, we have made some tests for a smaller density of cut bonds ($c = 0.15$), finding: stronger finite-size corrections, larger statistical fluctuations, and a smaller breaking range. The larger fluctuations are due to the smaller absolute number of cut bonds. Since, qualitatively speaking, we have not found significant differences, we have preferred to concentrate our efforts on the study of a single density of defects that could presumably allow more reliable results. For all the above reasons, the larger density $c = 0.3$ was found to be more convenient.

The only quantitative analysis we attempted for smaller c concerns the scaling behavior of N_b, for which we found a β value approximately equal to 1.27, i.e., smaller than in the previous case. This result is not suprising, as it is known that upon reducing the number of defects the fracture process becomes more localized.

Another parameter that we have modified is the threshold. Upon increasing it from 1.1 to 1.5 (i.e., by increasing the critical displacement by a factor of 5), we find that the critical strain passed from 0.0368 to 0.15, a value ''only'' four times larger: this is an indirect confirmation that nonlinear effects due to the lattice deformation are not negligible. Also the threshold changes yield to larger finite-size effects, which induced us to prefer the value 1.1 considered in the previous sections.

Finally, we replaced the harmonic potential with the more realistic nonlinear LJ potential. It is obvious that if the threshold distance is chosen too small we are back to the harmonic case, as the nonlinearity plays no role. For this reason, the threshold has been set equal to a larger value, namely, $d = 1.8$, above the inflection point, in the range where an increase of the deformation reduces the stress. The most detailed analysis was again performed for $c = 0.3$ in order to allow a meaningful comparison with the previous studies. The scenario emerging from Fig. 9, where the stress-strain curves are reported, is very reminiscent of that observed in Fig. 3. A surprising difference is that the initial behavior is more linear in this case than in the previous one. This is presumably due to a partial cancellation of the nonlinear effects following from the lattice deformation with those due to the interaction rule.

In spite of the larger threshold, the critical stress value is smaller than in the harmonic case. This is because the effect of the larger threshold is overcompensated by the stress reduction above the inflection point of the potential. On the other hand, the critical displacement ($d_c = 0.0318$) is close to the value found with harmonic springs. Moreover, the inset of Fig. 9 reveals a good overlap of the strain curves plotted versus Δ (in this case, the statistical uncertainty is approximately 10^{-3}, 5×10^{-4}, 3×10^{-4}, and 2×10^{-4} for $L = 10$, 20, 40, and 80, respectively) with the major exception of the data for the smallest lattice size ($L = 10$). Therefore, the fracture range again appears to remain finite in the thermody-

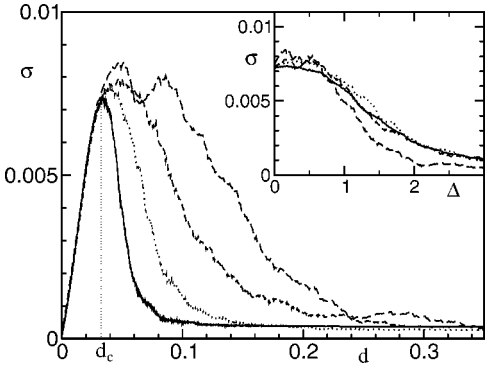

FIG. 9. Stress-strain curves reported as in Fig. 3, with reference to the Lennard-Jones potential. The critical strain here is $d_c = 0.0318$.

namic limit. This is completely confirmed by the plot in Fig. 10 of the integrated density of broken bonds, where one can again see a good overlap of the curves corresponding to $L = 20$, 40, and 80 (in this case, the statistical error is slightly larger than before, being approximately of the order of 3–4 %). The only region where the overlap is not equally good is the interval of negative Δ's, i.e., the initial part of the fracture. In the absence of theoretical arguments, we cannot decide whether this is due to larger finite-size corrections or to a cross over toward a different regime. In either case, such deviations do not contradict the hypothesis of a finite fracture range for $L \to \infty$ but might rather suggest the opposite.

The only apparently relevant difference that we have found from the harmonic potential concerns the tail of the probability distribution $Q(\Delta)$. From the data reported in Fig. 11, a power law seems to be more appropriate for describing the asymptotic behavior of $Q(\Delta)$. The power law means that larger strains can be sustained by the lattice before its final breakdown. This qualitative difference is likely to be attributable to the above mentioned nonlinear behavior of the LJ force field.

Finally, the growth rate β of N_b is slightly smaller than for harmonic springs, $\beta = 1.27 \pm 0.03$, and the same is true for the growth rate of $N_b^{(o)}$ ($\beta = 1.44 \pm 0.04$). Such differences

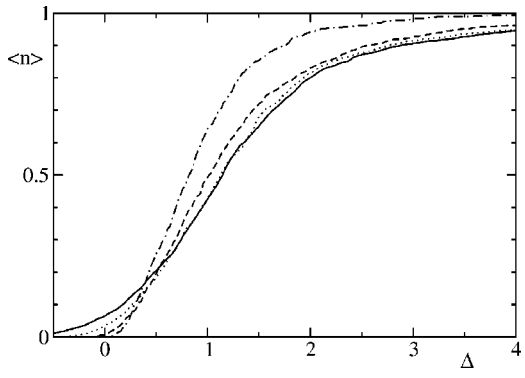

FIG. 10. The integrated probability distribution of broken bonds reported as in Fig. 5, with reference to the Lennard-Jones potential and with the same value of the critical strain d_c adopted in the previous figure.

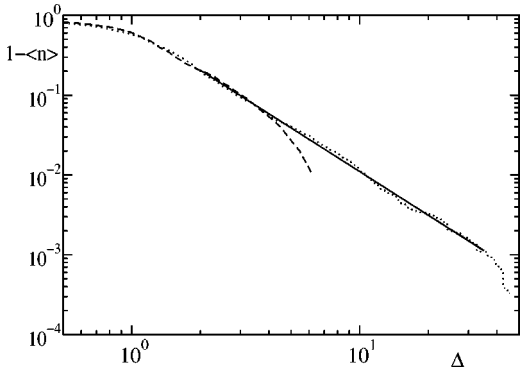

FIG. 11. Tail of the integrated probability distribution of broken bonds for $L = 80$: the dotted curve refers to the average fraction for fixed strain, while the dashed line refers to the average strain for fixed fraction of broken bonds. The slope of the straight line resulting from a power-law best fit is equal to 1.8. As for Fig. 5, we are unable to provide convincing estimates of the statistical error.

are suggestive of a continous dependence of β on c but are also compatible with different finite-size corrections.

VI. DISCUSSION AND SUMMARY

In this paper we have investigated several aspects of the onset of fractures in a two-dimensional model of a heterogeneous material in strain-controlled conditions. One of the questions that we considered concerns the probability distribution of broken bonds as a function of the applied strain. We found evidence that both in harmonic springs and in the Lennard-Jones potential the probability distribution $Q(\Delta)$ converges toward a smooth function for a suitable choice of the critical value d_c [see Eq. (4)]. We find that $Q(\Delta)$ develops an infinite tail on both the left and right sides. The left tail arises because the global strain corresponding to the first breakdown grows more slowly than linearly with the lattice size L [13]. Conversely, the right tail signals a faster-than-linear growth of the strain corresponding to the final breakdown. It is now highly desirable to develop even approximate but analytical arguments to establish the shape of $Q(\Delta)$.

As a further subject, we looked at the scaling behavior of the number of broken bonds, by grouping them into disjoint clusters. As a result, we found that, besides the major cluster, there exists an ensemble of microcracks that contains a small fraction of the overall number of broken bonds but, nevertheless, exhibits a faster growth rate. On the basis of our simulations, we predict that in sufficiently large lattices the opposite should be true, i.e., the majority of broken bonds should, in the thermodynamic limit, be found out of the major crack. It would be nice to see whether some crossover toward a different regime comes into play in larger lattices.

Finally, we want to comment on the fractal character exhibited by the major cluster. Various experimental studies performed in the last decade on different types of material have revealed the existence of two scaling regimes [3]: over small length scales $\zeta \approx 0.5$ (i.e., $D = 1.5$) while over somewhat larger scales $\zeta \approx 0.8$ ($D = 1.2$). These two regimes

seem to correspond to two different processes: the creation of distributed small areas of damage and the subsequent growth of the fracture path through the connection of such areas in a self-determined region of the sample. Additionally, the crossover between the two regimes appears to be connected with the existence of different fracture velocities. Our results qualitatively confirm such a scenario. In fact, for $c=0.3$, the growth rate β of broken bonds in the main crack is 1.31 and 1.27 in the harmonic and LJ potentials, respectively. Such values are slightly larger than the fractal dimension expected from the experimental results ($D=1.2$), but the difference can very well be attributed to finite-size corrections. Indeed, upon decreasing c, smaller β values were observed and it is altogether unlikely that the dimension D depends continuously on the concentration of defects. Again, simulations with larger lattices could help in clarifying this point, but, more than that, theoretical insight is needed to make further progress.

Furthermore, it is very tempting to compare the growth rate of the microcracks out of the main cluster with the exponent experimentally measured to characterize the fracture roughness over microscopic length scales. In this case, there is even an almost quantitative agreement, as we find 1.52 and 1.44 (in the harmonic and LJ potentials, respectively), to be compared with the experimental 1.5.

We can thus conclude that the model discussed in this paper appears to be sufficiently accurate to capture some of the relevant features that have been observed in fractures of real systems. It is now compelling both to modify the setup to allow further quantitative tests (see, for instance, the statistical analysis performed in Ref. [11] in the context of stress-controlled rather than strain-controlled fractures) and to start developing even approximate analytical arguments to put our results on firmer ground.

ACKNOWLEDGMENTS

We thank S. Ciliberto, S. Ruffo, and E. Bouchaud for fruitful discussions.

[1] B. B. Mandelbrot, *The Fractal Geometry of Nature* (Freeman, New York, 1982).
[2] B. B. Mandelbrot, D. E. Passoja, and A. J. Paullay, Nature (London) **308**, 721 (1984).
[3] E. Bouchaud, J. Phys.: Condens. Matter **9**, 4319 (1997), and references contained therein.
[4] P. Vashishta and A. Nakano, Comput. Sci. Eng. **1**, 20 (1999).
[5] *Fracture*, edited by H. Liebowitz (Academic Press, New York, 1986), Vols. I–VII.
[6] *Physical Metallurgy Principles*, edited by R. Reed-Hill (PWS Publishing Company, Boston, 1996).
[7] H. J. Herrmann and S. Roux, *Statistical Models for the Fracture of Disordered Media* (North-Holland, Amsterdam, 1990).
[8] G. Cannelli, R. Cantelli, and F. Cordero, Phys. Rev. Lett. **70**, 3923 (1993).
[9] A. Petri, G. Paparo, A. Vespignani, A. Alippi, and M. Costantini, Phys. Rev. Lett. **73**, 3423 (1994).
[10] J.-C. Amifrani, C. Le Floc'h, D. Sornette, and B. Souillard, J. Phys. I **5**, 631 (1995).
[11] A. Garcimartin, A. Guarino, L. Bellon, and S. Ciliberto, Phys. Rev. Lett. **79**, 3202 (1997).
[12] B. K. Chakrabarti, D. Chowdury, and D. Stauffer, Z. Phys. B: Condens. Matter **62**, 343 (1986).
[13] P. D. Beale and D. J. Srolovitz, Phys. Rev. B **37**, 5500 (1988).
[14] M. Born and K. Huang, *Dynamical Theory of Crystal Lattices* (Oxford University Press, New York, 1954).
[15] B. Kahng, G. G. Batrouni, S. Redner, L. de Arcagelis, and H. J. Herrmann, Phys. Rev. B **37**, 7625 (1988).
[16] A. Hansen, S. Roux, and H. J. Herrmann, J. Phys. (France) **50**, 733 (1989).
[17] L. De Arcangelis, A. Hansen, H. J. Herrmann, and S. Roux, Phys. Rev. B **40**, 877 (1989).
[18] G. N. Hasshold and D. J. Srolovitz, Phys. Rev. B **39**, 9273 (1989).
[19] A similar study was performed in [12] without, however, paying attention to the scaling properties of the two quantities.
[20] L. Bellon, Ph.D. thesis, Ecole Normale Supérieure, Lyon, 1998 (unpublished).
[21] S. Lepri, R. Livi, and A. Politi, Phys. Rev. Lett. **78**, 1896 (1997).
[22] L. M. Schwartz, S. Feng, M. F. Thorpe, and P. N. Sen, Phys. Rev. B **32**, 4607 (1985).
[23] D. J. Jacobs and M. F. Thorpe, Phys. Rev. E **53**, 3682 (1996).
[24] M. Zei, Tesi di Laurea, Università di Firenze, Firenze, 1997 (unpublished).
[25] D. Stauffer and A. Aharony, *Introduction to Percolation Theory* (Taylor & Francis, London, 1991).
[26] S. Roux, A. Hansen, H. Herrmann, and E. Guyon, J. Stat. Phys. **52**, 237 (1988).
[27] E. Louis and F. Guinea, Europhys. Lett. **3**, 871 (1987).
[28] A. Hansen, E. L. Hinrichsen, and S. Roux, Phys. Rev. B **43**, 665 (1991).
[29] G. Caldarelli, C. Castellano, and A. Vespignani, Phys. Rev. E **49**, 2673 (1994).
[30] G. Caldarelli, R. Cafiero, and A. Gabrielli, Phys. Rev. E **57**, 3878 (1998).